

Quantitative understanding of negative thermal expansion in scandium trifluoride from neutron total scattering measurements

Martin T. Dove^{1,2,3,*}, Juan Du³, Zhongsheng Wei³, David A. Keen⁴, Matthew G. Tucker⁵, and Anthony E. Phillips³


¹Schools of Computer Science and Physical Science & Technology, Sichuan University, Chengdu 610065, People's Republic of China

²Department of Physics, School of Sciences, Wuhan University of Technology, 205 Luoshi Road, Hongshan district, Wuhan, Hubei 430070, People's Republic of China

³School of Physics and Astronomy, Queen Mary University of London, Mile End Road, London E1 4NS, United Kingdom

⁴ISIS Facility, Rutherford Appleton Laboratory, Harwell Campus, Didcot, Oxfordshire OX11 0QX, United Kingdom

⁵Oak Ridge National Laboratory, Neutron Scattering Division, 1 Bethel Valley Road, Oak Ridge, Tennessee 37831, USA

 (Received 11 March 2020; revised 22 June 2020; accepted 27 July 2020; published 16 September 2020)

Negative thermal expansion (NTE)—the phenomenon where some materials shrink rather than expand when heated—is both intriguing and useful but remains poorly understood. Current understanding hinges on the role of specific vibrational modes, but in fact thermal expansion is a weighted sum of contributions from every possible mode. Here we overcome this difficulty by deriving a real-space model of atomic motion in the prototypical NTE material scandium trifluoride, ScF_3 , from total neutron scattering data. We show that NTE in this material depends not only on rigid unit modes—the vibrations in which the scandium coordination octahedra remain undistorted—but also on modes that distort these octahedra. Furthermore, in contrast with previous predictions, we show that the quasiharmonic approximation coupled with renormalization through anharmonic interactions describes this behavior well. Our results point the way towards a new understanding of how NTE is manifested in real materials.

DOI: [10.1103/PhysRevB.102.094105](https://doi.org/10.1103/PhysRevB.102.094105)

I. INTRODUCTION

Almost all materials expand when heated, but some shrink instead. This phenomenon of *negative thermal expansion* (NTE) [1–4] is of fundamental interest from a structural and thermodynamic point of view, and also commercially important [5–7], for instance in preparing substrates resistant to thermal shock. It is among the most widely studied of the anomalous negative thermodynamic properties, others including auxetics with negative Poisson's ratio [8] and materials which soften under pressure (negative derivative of the bulk modulus with pressure) [9–11].

At the present time we only have a *qualitative* understanding of the general principles underlying the origin of NTE arising from vibrational rather than magnetic or electronic reasons, based on an idea called the ‘tension effect’ [1,6,12]. We illustrate this idea in Fig. 1 for a linear arrangement of octahedral groups of atoms. Rotations of neighboring polyhedra will give rise to a transverse displacement of the shared vertex atom. If the bonds between the central and vertex atoms are strong, the transverse displacement of this atom, u , will pull its neighbors inwards rather than stretching

the bond. If these transverse motions arise from phonons of angular frequency ω , classical harmonic phonon theory gives $\langle u^2 \rangle = k_B T / m \omega^2$, where T is the temperature. By geometry, if the bonds do not change their length, the thermal motion reduces the lattice parameter a from a value a_0 at low temperature to $a \simeq a_0(1 - \langle u^2 \rangle / a_0^2) = a_0(1 + \alpha T)$, giving a negative value of the coefficient of linear thermal expansion, $\alpha = a^{-1} \partial a / \partial T = -k_B / m a_0^2 \omega^2$ [1].

This simple picture is far from a good explanation. For one thing, we have to add to this the effects of all other phonons, many of which (including the bond-stretching vibration) will contribute towards *positive* thermal expansion. The tension effect therefore requires that the associated phonons must represent a sufficiently significant number of the total number of phonons. Furthermore, the fragment of a structure shown in isolation in Fig. 1 is part of a three-dimensional crystal structure with the same type of connections in the other two directions. The connections to the rest of the structure give constraints that can significantly reduce the flexibility of the fragment and hence reduce the contribution of the tension

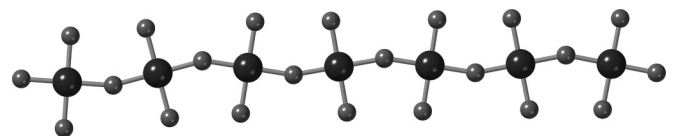


FIG. 1. Representation of a linear arrangement of corner-linked structural octahedra showing rotations. For clarity the upper atoms are not shown.

*martin.dove@icloud.com

effect to thermal expansion. For example, the modulation shown in Fig. 1 will require distortions of polyhedra linked in other directions, and in fact in the plane of the diagram there is only one modulation—the one in which neighboring polyhedra rotate in opposite senses of equal magnitude—that involves no distortions. The energy cost of polyhedral distortions may reduce the effect of such tension-effect vibrations. In view of this discussion, there is currently no physical understanding of why our subject material, ScF_3 , shows NTE, whereas almost every cubic perovskite material has positive thermal expansion, even though they all have the same basic network structure [13].

We present here an experimentally-based atomic-scale analysis of NTE in the prototypical material ScF_3 [14–16], obtained from neutron total scattering measurements analyzed using the reverse Monte Carlo (RMC) method. This approach is used to refine configurations of atoms so that both their long-range and their local structure are consistent with experimental data. While there have been a few reports of total scattering measurements of NTE materials [15,17–26]—including ScF_3 itself [15,26–29]—in only one previous case, namely that of ZrW_2O_8 [19,21], has the method been used to generate an atomic model of the fluctuations associated with NTE to provide a consistent examination of the tension effect. From our analysis of the atomic configurations across a wide range of temperatures generated in this study we show that the fluctuations associated with the tension effect are a mix of whole-body rotations and bond-bending distortions of ScF_6 octahedra. We have determined the relative balance of these in ScF_3 across the range of temperatures in our experiment and evaluated how this balance leads to NTE in ScF_3 , whereas similar materials such as SrTiO_3 show positive expansivity [30]. The picture that emerges here is consistent across the whole range of temperatures and supported by simulations using a model system. We also analyze the effects of anharmonicity in ScF_3 through the variation of the distribution of atomic displacements with temperature, given some recent calculations of single-model anharmonicity in ScF_3 [16], and our growing understanding that anharmonicity has the effect of reducing NTE at high temperatures [31,32]. Total scattering data analyzed using the reverse Monte Carlo method is the only way to obtain information about these issues from experiment.

II. BACKGROUND: RECIPROCAL-SPACE MODEL OF NEGATIVE THERMAL EXPANSION IN ScF_3

Scandium trifluoride, ScF_3 , has the rhenium trioxide structure, equivalent to the perovskite structure with a vacant A site (Fig. 2). It displays isotropic negative thermal expansion over the range 0 to 1100 K—our data are shown in Fig. 3—with a linear coefficient of thermal expansion of $\alpha = -10 \text{ MK}^{-1}$ at 200 K [14].

Accurate calculations of the phonon dispersion curves of ScF_3 using the density functional theory (DFT) method [16,32,33] show two important points. The first is that there is a line in reciprocal space (together with the symmetrically related lines) containing the lowest-energy phonons, namely for the wave vectors $(\frac{1}{2}, \frac{1}{2}, \xi)$ for $-\frac{1}{2} \leq \xi \leq \frac{1}{2}$; the two

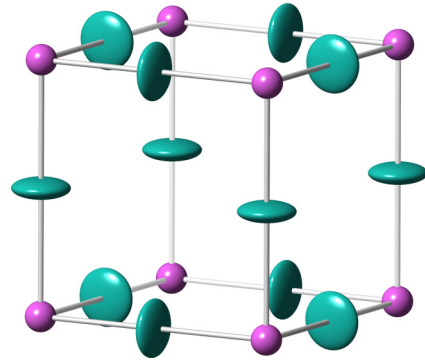


FIG. 2. Crystal structure of ScF_3 at a temperature of 1200 K obtained by Rietveld refinement of neutron powder diffraction data reported in this paper. It has a primitive cubic structure (Strukturbericht symbol $D0_9$, space group $Pm\bar{3}m$) with one formula unit per unit cell. The ellipsoids (Sc pink, F green) represent the thermal motion along different directions, with the volume enclosing 50% of the total distribution of atom positions.

special points $\xi = 0$ and $\xi = \frac{1}{2}$ have labels M and R , respectively. The eigenvectors of these modes correspond to transverse motions of the F atoms with whole-body rotations of the ScF_6 octahedra. Measurements of inelastic x-ray scattering [33] and diffuse x-ray scattering [34] from single crystals support this picture exactly. The second point is that the frequencies of phonons away from the M – R line increase rapidly with frequency, and these modes have low frequency *only* for wave vectors near this line in reciprocal space. Again, this point is consistent with the inelastic and diffuse scattering measurements [33,34].

The low-frequency modes with wave vectors along the M – R line and with eigenvectors corresponding to octahedral rotations are what are called rigid unit modes (RUMs) [1,35–38]. Their low energy is a consequence of the fact that the force constants associated with bending the octahedral F–Sc–F angles are much larger than those associated with bending the linear Sc–F–Sc angles; our estimate discussed in the Supplemental Material [39] is that the two force constants differ by a factor of around 50. Such a large factor accounts for the fact that the value of the frequency of the transverse acoustic mode at wave vector $(\frac{1}{2}, 0, 0)$ is much larger than that of the RUM frequency, seen in both the DFT calculations [16,32,33] and inelastic x-ray scattering experiments [33]. The same situation is seen in the experimental phonon dispersion curves of the cubic perovskite phase of SrTiO_3 [40]. The existence of RUMs provides a natural mechanism for the tension effect in NTE materials since the rotations give rise to a shrinkage of the crystal structure and these modes have the necessary low energy [1,37,38]. Indeed, the DFT calculations show that the RUMs have a considerably larger contribution to NTE than all other individual phonons, by two orders of magnitude [41].

As we have noted, pure RUMs exist along lines of wave vectors. A line of wave vectors of RUMs in ScF_3 occupies only a tiny—effectively infinitesimal—fraction of reciprocal space, and virtually all phonons must necessarily involve distortions of the ScF_6 octahedra. In particular, even though the pure RUM motions have the highest contribution to NTE

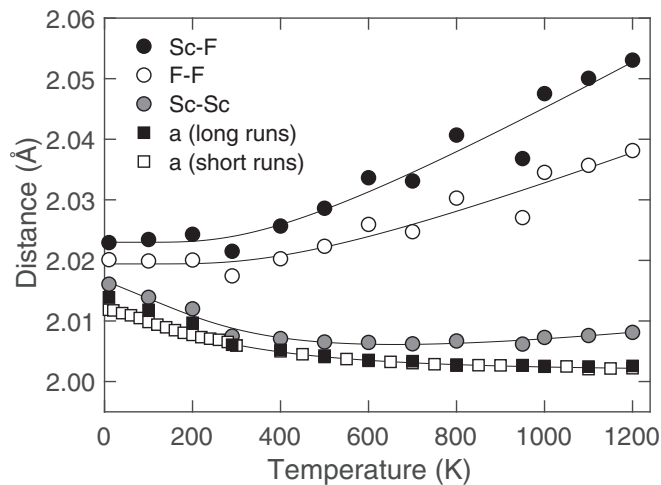


FIG. 3. Comparison of the temperature dependence of half the lattice parameter, $a/2$ (black squares, filled squares representing data from longer measurements and open squares representing data from shorter measurements), half of the average instantaneous nearest-neighbor Sc–Sc distance obtained from analysis of the RMC configurations (gray filled circles), the average instantaneous nearest-neighbor F–F distance obtained from analysis of the RMC configurations scaled by $1/\sqrt{2}$ (open black circles), and the average instantaneous nearest-neighbor Sc–F distance also obtained from analysis of the RMC configurations (black filled circles). In each plot statistical error bars are smaller than the sizes of the data symbols. The scaling means that each data set should converge to a value of $a/2$ at low temperature. The lines are guides to the eye; the guides for the F–F and Sc–F distances were obtained by fitting functions of the form $d = d_0 + \alpha \coth(\theta/T)$, and the guides for the lattice parameter and Sc–Sc distances were obtained by fitting functions of the form $d = d_0 - \gamma T + \alpha \coth(\theta/T)$, where the parameters d_0 , α , γ , and θ were variables in the fitting process.

of any phonon, their tiny weighting in reciprocal space means that any tension effect model must involve such distortions. The finite, as opposed to infinite, stiffness associated with distortions of the polyhedra are in fact an important part of the RUM model [38]; we return to this point in Sec. VIII. In fact, the DFT phonon calculations [16,32,33] show that in reciprocal space the tension effect will ‘bleed into’ the phonons whose wave vectors are close to, but not exactly on, the line M – R . These modes have a large component of rotation but an increasing component of polyhedral distortion on moving away from the M – R line in reciprocal space. They are, in effect, what we would call quasi-RUMs [36]. The extent to which the spectrum of quasi-RUMs can give rise to an overall NTE will depend on the extent to which the polyhedra can easily be distorted, a question that is analyzed in detail in this paper. This will give us a new perspective of the role of RUMs in the tension effect that will be applicable to many NTE materials and will enable us to understand why NTE can exist in some materials but not in other materials with close structural similarity.

At this point we note that the authors of Ref. [26] have proposed a radically different model. Their central idea is that the ScF_6 octahedra have no internal rigidity in terms of bending of the bonds and that the Sc–F bonds can rotate in

an uncorrelated way as independent Einstein oscillators. In part this idea is based on a misleading interpretation of the first three peaks in the pair distribution function because of the use of inappropriate integration limits coupled with the effects of noise associated with the Fourier transforms. The idea of the Sc–F bonds being able to rotate in an uncorrelated motion implies the absence of a force constant associated with bending of the octahedral F–Sc–F bond, which is directly the opposite of the RUM model. This type of model would surely give rise to a significant tension effect. However, it would lead to an excitation spectrum with six low-frequency modes for all wave vectors and an additional two low-frequency shear acoustic modes along the $(\xi, 0, 0)$ direction and one along the $(\xi, \xi, 0)$ direction. While this model of uncorrelated Sc–F motion is appealing as an intuitive interpretation of the tension effect, it is completely inconsistent with our knowledge of the phonon dispersion curves by both *ab initio* calculation [16,32,33] and inelastic x-ray scattering measurements [33]. A recent paper based on new x-ray total scattering measurements [29] supports the interpretation presented here, based on an earlier preprint of this paper, over the model of uncorrelated F-atom motions proposed in Ref. [26].

The RUM model with infinite stiffness and the uncorrelated model of Ref. [26] represent two opposite ends of a spectrum. We would argue that the calculated [16,32,33] and measured [33] phonon dispersion curves actually mean that the balance is more towards a RUM model with more polyhedral flexibility than found in corresponding oxides. Where ScF_3 actually sits in this balance is explored in detail in this paper.

III. METHODS

Neutron total scattering and diffraction experiments were performed on the Polaris diffractometer at the UK ISIS spallation neutron facility. The sample was obtained commercially, and x-ray and neutron powder diffraction measurements showed that the sample is of single phase within the limits of detection. The sample was packed into a cylindrical vanadium can of diameter 8 mm. Measurements for 750 μA h were obtained over the temperature range 10–1200 K, with shorter runs at intermediate temperatures performed for crystal structure analysis. The POLARIS instrument can measure down to a wavelength of 0.1 \AA [42], which gives a maximum energy transfer far in excess of the upper limit of 85 meV required from the DFT phonon calculations on ScF_3 [16], and therefore the experiments and subsequent analysis capture the full range of phonon excitations.

Rietveld refinement was carried out using the GSAS software [43] with the EXPGUI interface [44]. Data were prepared for Rietveld analysis using the MANTID software [45].

The RMC simulations were performed using the RMCprofile code [46]. The data sets used were the total scattering function after correction and subtraction of the self term, $i(Q)$, the pair distribution function (PDF) $D(r)$ obtained as Fourier transform of the function $Qi(Q)$ (the corrections to form $i(Q)$ and conversion to the PDF $D(r)$ were performed using the GUDRUN package [47]), and the Bragg scattering profile. Key equations and data are given in the Supplemental Material [39], showing the high quality of the fitting we were able to achieve. In addition to references cited in the main text here,

the Supplemental Material [39] also includes a citation of Ref. [48], which discusses and compares different formalisms for total scattering and pair distribution functions, including the definitions of our functions $i(Q)$ and $D(r)$.

Molecular dynamics simulations were performed using the DL_POLY code [49], using a model developed by fitting the calculated dispersion curves to the DFT results of Ref. [16] using the GULP lattice simulation code [50,51]. The model is described in more detail in Sec. VI, in the Supplemental Material [39], and in the parallel Ref. [11]. The Supplemental Material also includes a citation of Ref. [52], which discusses the method used for calculating and displaying mode Grüneisen parameters in calculated phonon dispersion curves.

IV. REAL-SPACE ANALYSIS OF NEGATIVE THERMAL EXPANSION

We collected total neutron scattering data from a powder sample of scandium trifluoride, measuring both the Bragg scattering—sensitive to the long-range order—and the diffuse scattering. Although several previous pair distribution function studies of ScF₃ have used x-rays [15,27–29], for our analysis neutron radiation was a more appropriate choice, for three reasons. First, the accessible range of scattering vector Q , and hence the resolution of the pair distribution function derived from it, is much greater: we were able to measure up to a maximum value of $Q_{\max} = 50 \text{ \AA}^{-1}$, while with x rays the maximum achievable value of Q with a short-wavelength silver anode is 22.5 \AA^{-1} and is usually practically up to around 30 \AA^{-1} with synchrotron radiation measurements. Second, the x-ray atomic form factor decays rapidly with scattering vector Q , which further limits the Q range in which useful data can be collected: even if we were somehow able to measure x-ray scattering at 50 \AA^{-1} , the scattering factor of Sc would be only 0.7% of its value at low Q . Finally, because this Q -dependence differs between atoms, calculating a scattering-weighted pair distribution function from a trial configuration of atoms is necessarily approximate.

Thus our neutron data enabled us to calculate high-resolution, bias-free pair distribution functions $D(r)$ (see Sec. III), which are effectively histograms of instantaneous interatomic distances. We then used the reverse Monte Carlo (RMC) method [46,53–55] to obtain a set of atomic configurations consistent with these data, each of which can be regarded as a plausible snapshot of the instantaneous atomic positions in this material.

The experimental lattice parameter is shown in Fig. 3, plotted as $a/2$, showing the NTE over the temperature range 0–1100 K and positive expansion at higher temperatures consistent with previous data [14]. In this figure we also compare the mean nearest-neighbor Sc–F and F–F distances, and half the mean Sc–Sc distance, all three obtained from analysis of the RMC configurations. The Sc–F and F–F distances are fully consistent with the positions of the peaks in the PDF data, but in the case of the Sc–Sc distance, the peak in the PDF overlaps with that from the second-neighbor F–F distribution and thus we cannot extract this directly from the raw data. The prediction from the tension effect is that the distance between mean positions of two bonded atoms should be shorter than the ac-

tual mean bond length, and indeed as expected the Sc–F bond and F–F distances show normal positive thermal expansion (Sc–F expansion coefficient $\alpha = +15 \text{ MK}^{-1}$), whereas $a/2$ decreases on heating defining the negative thermal expansion. This result for the Sc–F bond is consistent with two recent measurements of the PDF [15,26,56].

Figure 3 also shows the temperature dependence of the mean distance between neighboring Sc atoms. One might expect, given the locations of the Sc atoms, for this distance to reflect exactly the lattice parameter. However, although slight, we see a difference between these two quantities that grows on heating, with the Sc–Sc distance showing a slightly weaker dependence on temperature than for the linear dimensions of the crystal and a change to positive expansivity at a lower temperature. A similar effect was seen in Zn(CN)₂, where the (negative) expansivity of the Zn–Zn distance is less negative than the linear expansivity of the crystal [20]. In that case the difference is due to the fact that the primary mechanism for NTE is from the acoustic modes [57]. This is of course different to ScF₃, where the main NTE modes are rotational modes of optic character that lie along the edges of the Brillouin zone. However, by symmetry these modes transform into transverse acoustic modes as the wave vectors changes from the M – R line to zero, as seen in the dispersion curves reported in Refs. [16,58]. We propose that the behavior of the Sc–Sc distance may be associated with the growing acoustic mode character of the NTE phonons moving away from the M – R line; indeed, the bending of the F–Sc–F right angle can be associated with the transverse acoustic (shear) mode.

V. LOCAL STRUCTURAL DISTORTIONS FROM REVERSE MONTE CARLO ANALYSIS

We now consider the local atomic motions that are associated with NTE. The fact that the Sc–F bond shows positive thermal expansion implies that the tension effect will provide the mechanism. Thus we need to consider effects associated with transverse motions of the F atom and the extent to which this is correlated with the ScF₆ octahedra moving as nearly-rigid objects or distorting. Figure 4(a) shows the behavior of three angles with temperature: first the variance of Sc–F–Sc angles as they distort from the value of 180°, second the variance of the F–Sc–F angles as they distort from the ideal octahedral angle of 90°, and third the mean-square rotations of the ScF₆ octahedra (calculated using the GASP tool; see below). The largest fluctuation, by a significant margin, is for the Sc–F–Sc angle, which is primarily associated with the transverse motions of the F anion and is consistent with both the thermal ellipsoids seen in Fig. 2 and the role of the tension effect. The other two angles, namely of the ScF₆ octahedral rotations and the bending of the F–Sc–F bond, are actually very similar to each other. Thus the transverse motions of the F atoms as reflected in the Sc–F–Sc angles are achieved by both rotations and bond-bending deformations of the ScF₆ octahedra.

In Fig. 4(b) we show the details of an analysis performed using the GASP method, based on using geometric algebra to represent the rotations of polyhedral groups of atoms [59–61]. Given a set of bond vectors for an octahedron, \mathbf{r}_i , where i runs over all the centroid-vertex bonds, we can compare the vectors

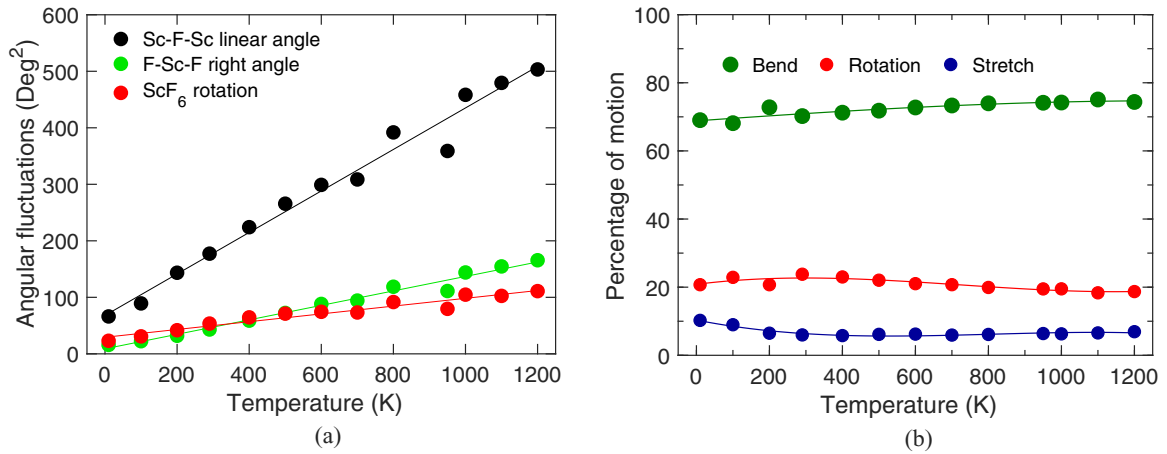


FIG. 4. (a) Comparison of the variances of three angles associated with local motions taken from the RMC configurations. The black points show the departure of the Sc–F–Sc angle from its nominal value of 180° , the green points show the variance of the F–Sc–F angle as it fluctuates from its nominal value of 90° , and the red points show the mean-square angle of rotation of the ScF₆ octahedra as a whole body. (b) Breakdown of the total motion (excluding overall polyhedral displacements) of the atoms in the ScF₃ crystal from the GASP analysis of the RMC configurations, where the red, green, and blue points and guides to the eye represent the fraction of the motion that is associated with whole-body rotations of the ScF₆ octahedra, deformations of the F–Sc–F right angles, and stretching of the Sc–F bonds, respectively. In both plots statistical error bars are smaller than the sizes of the data symbols, and the lines/curves are given as guides to the eye.

in one configuration with those in another (here, the ideal average structure), which we denote as \mathbf{r}' . The difference, which we call the *mismatch*, is $\mathbf{e}_i = \mathbf{r}_i - \mathbf{r}'_i$. GASP uses a least-squares algorithm to find the rotation of each octahedron that minimizes $M = \sum_i |\mathbf{e}_i|^2$, where we sum over all bonds in the polyhedron. The residual value of M per polyhedron is then decomposed into contributions from bending of bond angles and stretching of bonds, thereby accounting for the total motion involving nonuniform displacements of the F atoms. The results in Fig. 4(b) compare the extent to which the sum of the atomic motions of the F atoms in each ScF₆ octahedron can be separated into whole-body rotations of the octahedron, flexing of the F–Sc–F 90° bond angle, and stretching/shrinking of the Sc–F bonds [62]. This partition, which barely changes with temperature, is compared in summary form with corresponding results from a similar study of

TABLE I. The percentage mismatch between different atomic configurations of a network of MX₆ octahedra and the ideal structure, decomposed by GASP into X–M–X bending, M–X stretching, and MX₆ rotation components. We compare three systems: the RMC configurations of ScF₃, a hypothetical perovskite structure in the limit where the octahedra have flexible bond angles, and SrTiO₃ as also analyzed by RMC and taken from Ref. [63]. The hypothetical structure is an important comparison because, even if there are no rigidity constraints applied to the bond angles within the ScF₃ octahedra, some fraction of their random distortion will always be mathematically attributable to a rigid-body rotation.

Material	Bend	Stretch	Rotation
ScF ₃	70%	10%	20%
Flexible model	75%	5%	20%
SrTiO ₃	44%	19%	37%

the TiO₆ octahedra in the perovskite SrTiO₃ [63] in Table I, together with results from a molecular-dynamics simulation on a model system (described in the Supplemental Material [39]) in which the energy penalty for bending the X–M–X angle tends to zero. Our results show that ScF₃ is quite close to that limiting case [64]. The analysis suggests, therefore, that the ScF₆ octahedra in ScF₃ are significantly more flexible with regard to bending the anion-cation-anion angles than are the TiO₆ octahedra in SrTiO₃; we will argue below that this is the key difference that gives rise to NTE in ScF₃ but not in the cubic oxide perovskites [65].

Comparing absolute values of the fluctuations for ScF₃ and SrTiO₃ at a single temperature, say 300 K, we find that in SrTiO₃ the linear Ti–O–Ti angle fluctuates by an average of around 5° and the TiO₆ octahedra orientation fluctuates by around 2° [63], while the corresponding sizes of the fluctuations in ScF₃ are around 14° and 7° , respectively [Fig. 4(a)]. On the other hand, the coefficient of thermal expansion of the Ti–O bond, 10 MK^{-1} , is comparable to that of the Sc–F bond cited above, with similar Sc–F and Ti–O bond lengths.

We can also compare this analysis with the phonon dispersion curves for ScF₃ calculated using *ab initio* methods [16] and calculated for SrTiO₃ using a shell model fitted to inelastic neutron scattering and infrared spectroscopy [40]. We see that the octahedral cation-anion stretching frequencies are very similar (20 THz in ScF₃ and 22 THz in SrTiO₃), suggesting (given the similar masses of O and F) that the bonds in ScF₃ and SrTiO₃ are of similar stiffness. In both ScF₃ and SrTiO₃ the octahedral rigid-body rotational phonons between the R and M wave vectors are of very low frequency compared to the stretching mode in both materials, namely between 0.6 to 1.2 THz in ScF₃ and between 1.3 to 2.5 THz in SrTiO₃ at a temperature of 200 K. However, the bending frequencies are different. If we take, for example, the transverse acoustic mode frequency at X , $(\frac{1}{2}, 0, 0)$, which is a

shear mode that reflects bending distortions of the octahedra, we find that it is lower in frequency by around a factor of 2 in ScF_3 than in SrTiO_3 , meaning the corresponding force constants are four times smaller. This is consistent with our finding that the ScF_6 octahedra are rather more flexible than the TiO_6 octahedra. But care is needed not to go to the extreme viewpoint and imagine that there is no force constant associated with the bending of the F–Sc–F right angle. There is, and it directly gives rise to a nonzero shear elastic constant [66].

VI. MOLECULAR DYNAMICS SIMULATIONS WITH A SIMPLIFIED MODEL

Simulation methods can often give insights into the relationship between the properties of materials and their atomic structure. For ScF_3 there have been a number of simulation studies using the molecular dynamics (MD) method with classical force fields or *ab initio* methods [67–69]. What is less useful about such methods is that it is not easy to change parameters that directly affect one type of structure flexibility alone. Any change in some aspect of the model will affect everything. To address the question of the relative roles of the forces associated with the bending of the octahedral F–Sc–F bond angle or linear Sc–F–Sc bond angle we need to work with a simpler idealized model, and we explore this now.

The model introduced briefly in the previous section, and in our parallel paper on pressure-induced softening in ScF_3 [11], is described in more detail in the Supplemental Material [39]. The model has been designed and analyzed to see the effect of various independent parameters on the NTE. There are two parameters that are of interest (a third parameter controls the bond stretching, which is tuned to a high stiffness by comparison with the DFT phonon calculations). The first, with symbol A , controls flexing of the linear Sc–F–Sc bond and determines the frequency of the RUM along the M – R wave vectors. The value of this parameter was tuned directly by comparison of the calculated RUM frequencies with those given by the DFT phonon calculations. The second, with symbol k , controls flexing of the F–Sc–F right-angle, and its value was tuned to reflect the frequencies of the shear acoustic modes from the DFT dispersion curves. Increasing both of these parameters will reduce the flexibility of the structure in their respective ways and hence change the thermal expansion. We explicitly do not include ionic charges in the model because Coulomb interactions will affect the flexibilities of both the linear Sc–F–Sc bond and right-angle F–Sc–F bond. Nevertheless, the simple three-parameter model does a surprisingly good job of reproducing the phonon dispersion curves, comparing Fig. S11 with the results, say, of Ref. [16].

Figure 5 shows the results of varying both force constants starting from the model that best reproduces the DFT phonon dispersion curves. The first result from the data shown in Fig. 5 is that increasing both force constants will reduce the negative thermal expansion and eventually drive it positive. Increasing the F–Sc–F force constant k will increase the frequencies of the modes close to the RUM M – R line, which will reduce the number of phonons contributing significantly to the overall NTE and hence leading to a reduction and eventual elimination of NTE. This is consistent with the narrative

developed based on the RMC results presented above. On the other hand, the force constant associated with the linear Sc–F–Sc bond, A , plays a role in increasing the frequencies of the RUMs but less of a role in shaping the dispersion curves, so will have a gradual effect in changing the NTE as the mode frequencies increase. The increased frequency of the RUMs will lead to a reduced transverse amplitude of the F atoms. In some ways, this is similar to the effects of the forces imparted in the analogous perovskites with an atom in the **A** site (such as Sr in SrTiO_3). There is, however, one significant difference with regard to changing the two force constants. In the case of the F–Sc–F right angle, NTE vanishes by increasing the force constant value by a factor of 3.3, whereas in the case of the Sc–F–Sc angle, NTE vanishes by increasing the force constant value by around a factor of 40. Looking at dispersion curves in perovskites, for example in SrTiO_3 [40], suggests that in perovskites the size of this factor is not reached. On the other hand, the factor of 3.3 increase in the bending force constant is exactly consistent with the difference between ScF_3 and SrTiO_3 discussed in the previous section. Thus the difference strongly suggests that key effect in determining NTE is indeed the bond-bending flexibility of the ScF_3 octahedra.

VII. ANHARMONICITY

There is a lot of current interest in the role of anharmonic phonon interactions in NTE. Typically the most important ones are those involving fourth-order interactions, which have the effect of changing phonon frequencies. Several recent papers have studied anharmonicity in ScF_3 in various ways [16,32,33,70].

In renormalized phonon theory [71] the temperature dependence of a phonon angular frequency $\omega(\mathbf{k}, j)$ (j labels the mode for any \mathbf{k}) in the high- T limit varies as [32,72]

$$\omega^2(\mathbf{k}, j) = \omega_0^2(\mathbf{k}, j) + \frac{1}{2}k_B T \sum_{\mathbf{k}', j'} \frac{\alpha_4(\mathbf{k}, \mathbf{k}', j, j')}{\omega_0^2(\mathbf{k}', j')},$$

where ω_0^2 is the square of the harmonic angular frequency, and the interactions characterized by the fourth-order anharmonic parameters α_4 couple the phonon $(\pm\mathbf{k}, j)$ to all other phonons $(\pm\mathbf{k}', j')$. This summation includes the case $(\mathbf{k}, j) = (-\mathbf{k}', j')$; when this case is taken alone, it represents the *independent-mode approximation*. It is this approximation *only* that is probed in a frozen-phonon calculation [16], and it will give just a small part of the overall picture. That is, the contributions from the modes $(\mathbf{k}, j) \neq (-\mathbf{k}', j')$ are normally much more important than only the modes $(\mathbf{k}, j) = (-\mathbf{k}', j')$ in determining how phonon frequencies change with temperature. The DFT calculations of Li *et al.* [16] suggested that for the R -point mode the independent-mode anharmonic potential is quite large compared to the harmonic potential, but the summation over all modes may still mean that the primary anharmonic effects come instead from interactions across the Brillouin zone. Van Roekeghem *et al.* [70] recently studied the anharmonicity using both x-ray inelastic scattering and through calculations of the phonon frequencies via a renormalized phonon method. They showed, consistent with most perovskites, that the low frequency branch along the line M – R and the three lowest-frequency optic modes at zero

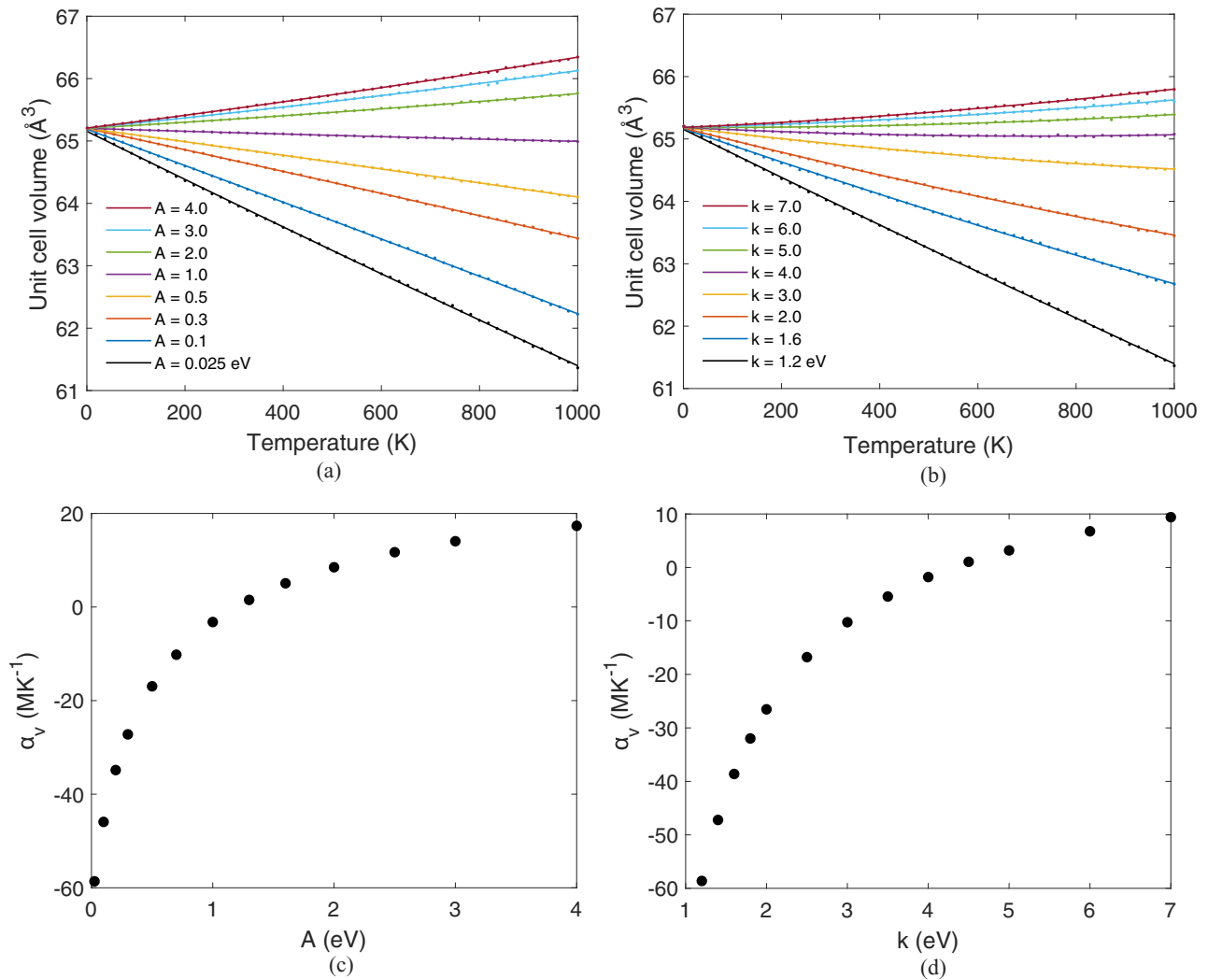


FIG. 5. (a) and (b) show the variation of volume of one unit cell of ScF₃ with the interoctahedral Sc–F–Sc and intraoctahedral F–Sc–F angle force constants, respectively, A and k (see Supplemental Material [39] for the equations). (c) and (d) show the corresponding coefficients of volumetric thermal expansivity for the cases $k = 1.2$ eV and $A = 0.025$ eV respectively, corresponding to the values that give best match to the DFT dispersion curves [16] as discussed in the Supplemental Material [39].

wave vector soften on cooling, consistent with renormalized phonon theory, whereas the higher-frequency modes harden on cooling. Similar results were obtained by Oba *et al.* [32]. The softening on cooling arises from direct anharmonic interactions via renormalized phonon theory as described here, whereas the hardening of the high-frequency modes arises primarily from thermal expansion of the Sc–F bond. In this model, the renormalized phonons continue to look like phonons with well-defined frequencies, with lifetimes substantially larger than the phonon frequency (see Fig. 3 of Ref. [70]). Separately, in Ref. [31] we showed from simple considerations that anharmonic renormalization of phonon frequencies will cause NTE to shift towards positive expansivity at higher temperatures; the same result is obtained by more detailed renormalized phonon theory calculations [32,70].

We have analyzed our RMC configurations to look for any effects of anharmonicity in the distributions of transverse displacements of fluorine atoms. This particular atomic displacement was chosen since it is active in the R -point RUM previously identified as having a dominant fourth-order term.

Figure 6 shows the distribution of these displacements of F atoms away from the Sc–Sc line as a function of temperature. Two features of these data are noteworthy. First, the distributions are well fitted by Gaussian functions at all temperatures. In particular, we find no evidence for a toroidal distribution of fluorine atoms, as conjectured in a recent PDF study [26,73]. Second, the fitted variance of these Gaussian distributions increases linearly with temperature, exactly as one would expect for a harmonic oscillator. We conclude that, to the extent to which anharmonicity is important in this material, it is *completely* described within the renormalized phonon approximation taken to fourth order. In other words, although fourth-order interactions seen by individual phonon modes may limit their amplitude at high temperature, there is an insufficient number of such modes with near-zero harmonic terms to make an appreciable difference to the distribution of atomic positions. Thus overall the most important anharmonic interactions involve couplings between different phonons, as described by the renormalized phonon approximation taken to fourth order rather than the independent mode approximation.

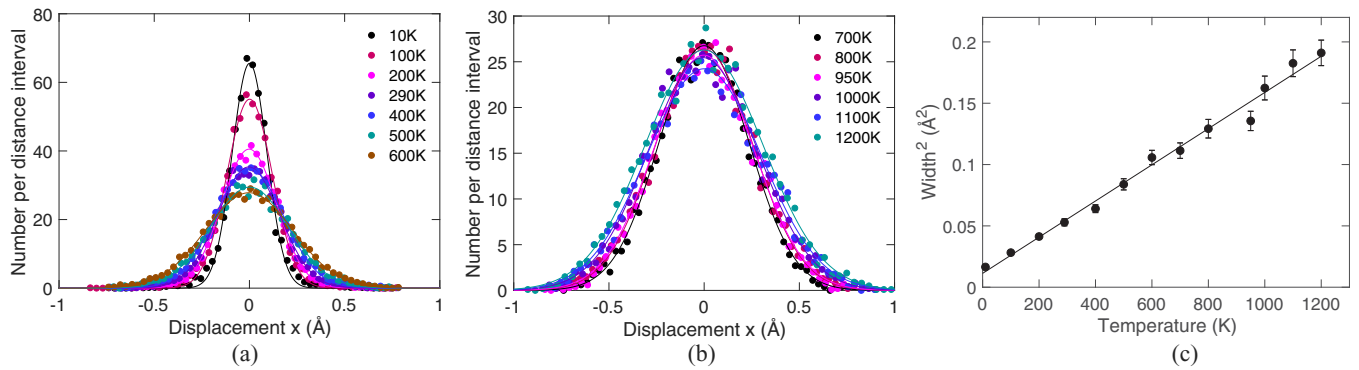


FIG. 6. (a) and (b) show histograms of the lateral displacements of the F atoms at the different temperatures (circles). At all temperatures the distributions are well described by Gaussian functions (thin lines). (c) shows the variance of the Gaussian fits as a function of temperature. The data follow a linear dependence on temperature throughout the range studied, as indicated by the fitted straight line, demonstrating that a renormalized phonon model is sufficient to describe the anharmonic effects in ScF_3 .

Furthermore, our results also rule out the significance of higher-order terms because they too would lead to a different temperature dependence.

It is worth making a general comment here. It is very tempting to assume that because high temperatures lead to large-amplitude motions, they also lead to significant and unusual anharmonic effects. Actually this need not be so, given that large amplitudes are perfectly possible within the harmonic approximation. Our analysis here shows that high temperature does not necessarily produce unusual behavior, such as envisaged in Ref. [26] for example. Instead, at high temperature ScF_3 behaves as a typical harmonic crystal, or at least as one whose behavior is only weakly perturbed by anharmonic effects. A similar conclusion was obtained from an RMC study of BiFeO_3 based on neutron total scattering data; in spite of very large atomic motions at high temperature, the average structure remains robustly constant across a wide range of temperatures and there are no unusual changes in atom distributions [74].

VIII. DISCUSSION AND CONCLUSIONS

Our two key conclusions from the analysis of the RMC configurations discussed above are that the NTE arises from a set of phonons with wave vectors around the lines of RUMs in reciprocal space and which are sufficiently extensive because of the relatively lower force constants associated with bending the bonds within the ScF_6 coordination octahedra than in related systems, and that the transverse displacement of the F atoms, although associated with a quartic mode, can be well described by a Gaussian distribution whose width varies linearly with temperature, consistent with a renormalized harmonic phonon model. These results are closely related, since the RUMs are exactly the modes that will have small quadratic terms and in which the quartic terms are thus expected to be dominant. What they show is that the quasi-RUM vibrations make dominant contributions to the thermal expansion, and in particular to the NTE, of ScF_3 . A similar conclusion was reached by the authors of Ref. [29] by a different type of analysis.

We need to state clearly that the deformations of the ScF_6 octahedra allowed within the quasi-RUMs do not in any way repudiate the importance of RUMs. It is a common misconception that the RUM model requires the octahedra to be very rigid (a mistake propagated in Ref. [26]), but in fact quite the opposite is true, as has been discussed in detail recently in Ref. [38]. The basic RUM model has always considered the structural polyhedra to have *finite*, rather than infinite, rigidity, which in the original application of the RUM model to displacive phase transitions is directly associated with the phase transition temperature [75–79]. In the same vein, the RUM model itself does not presuppose that any rigidity of the polyhedra arises only from covalent bonding. Polyhedral rigidity certainly can arise from Coulomb interactions or steric hindrance effects between anions within the structural polyhedra. In this sense our work here is also consistent with the viewpoint of Ref. [80], which discusses RUMs and quasi-RUMs in the context of a model with ionic forces.

The point is this: the fact that the RUMs are restricted to wave vectors lying on lines in reciprocal space means that they are a vanishingly small fraction of the total number of phonon modes and therefore alone they cannot give overall NTE. Instead, to get overall NTE it is necessary that there is a sufficiently-large number of low-frequency RUM-like phonon modes—quasi-RUMs—close to the wave vectors of the RUMs. This is possible if the polyhedra (in this case the ScF_6 octahedra) have some flexibility. Thus we propose firstly that the existence of the RUMs gives a set of phonons with the necessary low frequencies and appropriate mode eigenvectors for the tension effect to give NTE, and secondly that the flexibility of the polyhedra allows the contribution from the quasi-RUMs to spread across a sufficiently large volume in reciprocal space to have enough thermodynamic weighting to give an overall NTE. This explains concisely why there is NTE in ScF_3 but only positive thermal expansion in other perovskites such as SrTiO_3 ; both materials have stiff cation-anion (Sc–F or Ti–O) bonds, but the TiO_6 octahedra are more resistant to bond-bending distortion than the ScF_6 octahedra. This interpretation provides a plausible and reasonable explanation of the origin of NTE in ScF_3 : one that is predictive, that is based on standard concepts in condensed matter

physics, and that is consistent with previous experimental data and simulations.

In conclusion, our real-space analysis of ScF_3 , based on using the reverse Monte Carlo method with neutron total scattering data to generate configurations of atoms over a wide range of temperatures, has allowed us to establish a quantitative view of the structural fluctuations associated with NTE. Comparison with a similar study of SrTiO_3 , together with comparisons of published phonon dispersion curves, shows the importance of RUMs in giving rise to NTE, but that it is also necessary to have some degree of polyhedral distortion to spread the contributions to NTE across a wider range of wave vectors than those associated with the pure RUMs. Fluorinated octahedra have bonds that are as stiff as in their oxygenated counterparts but have more bond-bending flexibility. On this basis we suggest that in the search for materials with large negative coefficients of thermal expansion, fluorinated analogues of other oxides with NTE—one example being ZnF_2 as an analog of the rutile phase of TiO_2 [81]—might prove to be particularly fertile [82].

Original data sets are available directly from ISIS with Digital Object Identifier 10.5286/ISIS.E.RB1510519 [83]. Corrected data and atomic configurations are available on request from the corresponding author.

ACKNOWLEDGMENTS

We are grateful to ISIS for provision of neutron beam time, supported under Proposal No. RB1510519. We also appreciate help from Helen Playford (ISIS) in preparation for the experimental beam time. J.D. is grateful to the China Scholarship Council and Queen Mary University of London for financial support. This research utilized the following computing resources: (a) Queen Mary's Apocrita HPC facility (DOI: 10.5281/zenodo.438045), supported by QMUL Research-IT and funded by EPSRC Grants No. EP/K000128/1 and No. EP/K000233/1 (M.T.D.); (b) Midlands Plus Tier-2 HPC facility, funded by EPSRC Grant No. EP/P020232/1 (M.T.D.).

-
- [1] M. T. Dove and H. Fang, Negative thermal expansion and associated anomalous physical properties: Review of the lattice dynamics theoretical foundation, *Rep. Prog. Phys.* **79**, 066503 (2016).
- [2] J. Chen, L. Hu, J. Deng, and X. Xing, Negative thermal expansion in functional materials: Controllable thermal expansion by chemical modifications, *Chem. Soc. Rev.* **44**, 3522 (2015).
- [3] C. Lind, Two decades of negative thermal expansion research: Where do we stand? *Materials* **5**, 1125 (2012).
- [4] C. P. Romao, K. J. Miller, C. A. Whitman, M. A. White, and B. A. Marinkovic, Negative thermal expansion (thermomiotic) materials, in *Comprehensive Inorganic Chemistry II: From Elements to Applications* (Elsevier, Oxford, 2013), pp. 127–151.
- [5] K. Takenaka, Negative thermal expansion materials: Technological key for control of thermal expansion, *Sci. Technol. Adv. Mater.* **13**, 013001 (2012).
- [6] G. D. Barrera, J. A. O. Bruno, T. H. K. Barron, and N. L. Allan, Negative thermal expansion, *J. Phys.: Condens. Matter* **17**, R217 (2005).
- [7] Er-Jun Liang, Negative thermal expansion materials and their applications: A survey of recent patents, *Recent Patents on Mater. Sci.* **3**, 106 (2010).
- [8] X. Ren, R. Das, P. Tran, T. D. Ngo, and Y. M. Xie, Auxetic metamaterials and structures: A review, *Smart Mater. Struct.* **27**, 023001 (2018).
- [9] H. Fang and M. T. Dove, Pressure-induced softening as a common feature of framework structures with negative thermal expansion, *Phys. Rev. B* **87**, 214109 (2013).
- [10] H. Fang, A. E. Phillips, M. T. Dove, M. G. Tucker, and A. L. Goodwin, Temperature-dependent pressure-induced softening in $\text{Zn}(\text{CN})_2$, *Phys. Rev. B* **88**, 144103 (2013).
- [11] Z. Wei, L. Tan, G. Cai, A. E. Phillips, I. da Silva, M. G. Kibble, and M. T. Dove, Colossal Pressure-Induced Softening in Scandium Fluoride, *Phys. Rev. Lett.* **124**, 255502 (2020).
- [12] R. Mittal, M. K. Gupta, and S. L. Chaplot, Phonons and anomalous thermal expansion behavior in crystalline solids, *Prog. Mater. Sci.* **92**, 360 (2018).
- [13] It may be argued that since, in comparison with the perovskite structure, ScF_3 has no A-site cation, it should have more flexibility for rotational motions and hence for the tension effect to operate. However, this is a real-space intuition that doesn't necessarily correspond directly with what is really found. Since vibrations are correctly resolved into a summation of normal modes with wave vectors in reciprocal space, any effects of the A-site cation should be interpreted in terms of their effect on the frequencies of the relevant phonon modes. Here we see that the effect is not to block the motion at all. First, comparing for ScF_3 [16, 32, 33] and SrTiO_3 [40] the values of the lowest-frequency modes along the M - R directions in reciprocal space, as defined later, we find very similar frequency values and hence the capacity for similar RUM amplitudes. Furthermore, in many cubic perovskites there is a softening of the RUM phonon frequencies on cooling towards a displacive phase transition, which will increase the RUM amplitude.
- [14] B. K. Greve, K. L. Martin, P. L. Lee, P. J. Chupas, K. W. Chapman, and A. P. Wilkinson, Pronounced negative thermal expansion from a simple structure: Cubic ScF_3 , *J. Am. Chem. Soc.* **132**, 15496 (2010).
- [15] L. Hu, J. Chen, A. Sanson, H. Wu, C. Guglieri Rodriguez, L. Olivi, Y. Ren, L. Fan, J. Deng, and X. Xing, New insights into the negative thermal expansion: Direct experimental evidence for the “Guitar-String” effect in cubic ScF_3 , *J. Am. Chem. Soc.* **138**, 8320 (2016).
- [16] C. W. Li, X. Tang, J. A. Muñoz, J. B. Keith, S. J. Tracy, D. L. Abernathy, and B. Fultz, Structural Relationship between Negative Thermal Expansion and Quartic Anharmonicity of Cubic ScF_3 , *Phys. Rev. Lett.* **107**, 195504 (2011).
- [17] S. J. Hibble, S. M. Cheyne, A. C. Hannon, and S. G. Eversfield, Beyond Bragg scattering: The structure of AgCN

- determined from total neutron diffraction, *Inorg. Chem.* **41**, 1042 (2002).
- [18] S. J. Hibble, S. M. Cheyne, A. C. Hannon, and S. G. Eversfield, CuCN: A polymorphic material. Structure of one form determined from total neutron diffraction, *Inorg. Chem.* **41**, 4990 (2002).
- [19] M. G. Tucker, A. L. Goodwin, M. T. Dove, D. A. Keen, S. A. Wells, and J. S. O. Evans, Negative Thermal Expansion in ZrW_2O_8 : Mechanisms, Rigid Unit Modes, and Neutron Total Scattering, *Phys. Rev. Lett.* **95**, 255501 (2005).
- [20] K. W. Chapman, P. J. Chupas, and C. J. Kepert, Direct observation of a transverse vibrational mechanism for negative thermal expansion in $\text{Zn}(\text{CN})_2$: An atomic pair distribution function analysis, *J. Am. Chem. Soc.* **127**, 15630 (2005).
- [21] M. G. Tucker, D. A. Keen, J. S. O. Evans, and M. T. Dove, Local structure in ZrW_2O_8 from neutron total scattering, *J. Phys.: Condens. Matter* **19**, 335215 (2007).
- [22] M. Dapiaggi, H. J. Kim, E. S. Božin, S. J. L. Billinge, and G. Artioli, Study of the negative thermal expansion of cuprite-type structures by means of temperature-dependent pair distribution function analysis: Preliminary results, *J. Phys. Chem. Solids* **69**, 2182 (2008).
- [23] K. W. Chapman and P. J. Chupas, Anomalous thermal expansion of cuprites: A combined high resolution pair distribution function and geometric analysis, *Chem. Mater.* **21**, 425 (2009).
- [24] S. J. Hibble, A. M. Chippindale, E. Marelli, S. Kroeker, V. K. Michaelis, B. J. Greer, P. M. Aguiar, E. J. Bilbé, E. R. Barney, and A. C. Hannon, Local and average structure in zinc cyanide: Toward an understanding of the atomistic origin of negative thermal expansion, *J. Am. Chem. Soc.* **135**, 16478 (2013).
- [25] F. Bridges, T. Keiber, P. Juhas, S. J. L. Billinge, L. Sutton, J. Wilde, and G. R. Kowach, Local Vibrations and Negative Thermal Expansion in ZrW_2O_8 , *Phys. Rev. Lett.* **112**, 045505 (2014).
- [26] D. Wendt, E. Bozin, J. Neufeind, K. Page, W. Ku, L. Wang, B. Fultz, A. V. Tkachenko, and I. A. Zaliznyak, Entropic elasticity and negative thermal expansion in a simple cubic crystal, *Sci. Adv.* **5**, eaay2748 (2019).
- [27] C. Yang, P. Tong, J. C. Lin, X. G. Guo, K. Zhang, M. Wang, Y. Wu, S. Lin, P. C. Huang, W. Xu, W. H. Song, and Y. P. Sun, Size effects on negative thermal expansion in cubic ScF_3 , *Appl. Phys. Lett.* **109**, 023110 (2016).
- [28] L. Hu, F. Qin, A. Sanson, L.-F. Huang, Z. Pan, Q. Li, Q. Sun, Lu Wang, F. Guo, U. Aydemir, Y. Ren, C. Sun, J. Deng, G. Aquilanti, J. M. Rondinelli, J. Chen, and X. Xing, Localized symmetry breaking for tuning thermal expansion in ScF_3 nanoscale frameworks, *J. American Chem. Soc.* **140**, 4477 (2018).
- [29] T. A. Bird, J. Woodland-Scott, L. Hu, M. T. Wharmby, J. Chen, A. L. Goodwin, and M. S. Senn, Anharmonicity and scissoring modes in the negative thermal expansion materials ScF_3 and CaZrF_6 , *Phys. Rev. B* **101**, 064306 (2020).
- [30] The authors of Ref. [16] give a slightly misleading qualitative opinion on the flexibility of the ScF_6 octahedra on the basis of *ab initio* molecular dynamics simulations, because they constructed their atomic configuration with an *odd* number of unit cells along each direction. This choice automatically excludes all rigid unit modes, and thus their simulation is unrealistic and their conclusions, albeit qualitative, are affected by this choice.
- [31] H. Fang, M. T. Dove, and A. E. Phillips, Common origin of negative thermal expansion and other exotic properties in ceramic and hybrid materials, *Phys. Rev. B* **89**, 214103 (2014).
- [32] Y. Oba, T. Tadano, R. Akashi, and S. Tsuneyuki, First-principles study of phonon anharmonicity and negative thermal expansion in ScF_3 , *Phys. Rev. Mater.* **3**, 033601 (2019).
- [33] S. U. Handunkanda, E. B. Curry, V. Voronov, A. H. Said, G. G. Guzmán-Verri, R. T. Brierley, P. B. Littlewood, and J. N. Hancock, Large isotropic negative thermal expansion above a structural quantum phase transition, *Phys. Rev. B* **92**, 134101 (2015).
- [34] S. U. Handunkanda, C. A. Occhialini, A. H. Said, and J. N. Hancock, Two-dimensional nanoscale correlations in the strong negative thermal expansion material ScF_3 , *Phys. Rev. B* **94**, 214102 (2016).
- [35] A. P. Giddy, M. T. Dove, G. S. Pawley, and V. Heine, The determination of rigid-unit modes as potential soft modes for displacive phase transitions in framework crystal structures, *Acta Crystallogr., Sect. A: Found. Crystallogr.* **49**, 697 (1993).
- [36] K. D. Hammonds, M. T. Dove, A. P. Giddy, V. Heine, and B. Winkler, Rigid-unit phonon modes and structural phase transitions in framework silicates, *Am. Mineral.* **81**, 1057 (1996).
- [37] V. Heine, P. R. L. Welche, and M. T. Dove, Geometrical origin and theory of negative thermal expansion in framework structures, *J. Am. Ceram. Soc.* **82**, 1793 (1999).
- [38] M. T. Dove, Flexibility of network materials and the Rigid Unit Mode model: A personal perspective, *Philos. Trans. R. Soc., A* **377**, 20180222 (2019).
- [39] See Supplemental Material at <http://link.aps.org/supplemental/10.1103/PhysRevB.102.094105> for details of the Rietveld refinements and results; formalism of total scattering and pair distribution function; details of the reverse Monte Carlo method and graphs of the fitting to experimental data; and details of the flexibility model studied by the molecular dynamics simulation method.
- [40] W. G. Stirling, Neutron inelastic scattering study of the lattice dynamics of strontium titanate: Harmonic models, *J. Phys. C* **5**, 2711 (1972).
- [41] It is worth remarking about the origin of the stiffness in the structural polyhedra in general and more specifically in the case of the ScF_6 octahedra in ScF_3 . Much of the original literature on RUMs concerned silica and silicates, which are conventionally considered to have strong covalent bonds defining the shape and stiffness of the structural SiO_4 tetrahedra. However, it is important to understand that the rigidity of structural polyhedra do not rely on covalent bonding, because tension within the polyhedra in a system where the bonding is more ionic in nature can arise from mutual repulsions between the vertex ions because of size effects and Coulomb interactions. This is pertinent for ScF_3 . The Sc–F bond is relatively strong, as evidenced by the large value of the Sc–F stretching frequency in the phonon dispersion curves [16, 33, 32], indicating some degree of covalent bonding, but it is more likely that the ionic size and electrostatic interactions will be most important in the F–Sc–F bond-bending forces.
- [42] Polaris technical information, STFC ISIS Neutron and Muon Source, <https://www.isis.stfc.ac.uk/pages/polaris-technical-information.aspx> (2019).

- [43] A. C. Larson and R. B. Von Dreele, General Structure Analysis System (GSAS), Tech. Rep. LAUR 86-748 (Los Alamos National Laboratory, 2004).
- [44] B. H. Toby, EXPGUI, a graphical user interface for GSAS, *J. Appl. Crystallogr.* **34**, 210 (2001).
- [45] O. Arnold, J. C. Bilheux, J. M. Borreguero, A. Buts, S. I. Campbell, L. Chapon, M. Doucet, N. Draper, R. F. Leal, M. A. Gigg, V. E. Lynch, A. Markvardsen, D. J. Mikkelsen, R. L. Mikkelsen, R. Miller, K. Palmen, P. Parker, G. Passos, T. G. Perring, P. F. Peterson, S. Ren, M. A. Reuter, A. T. Savici, J. W. Taylor, R. J. Taylor, R. Tolchenov, W. Zhou, and J. Zikovsky, Mantid—Data analysis and visualization package for neutron scattering and μ SR experiments, *Nucl. Instrum. Methods Phys. Res., A* **764**, 156 (2014).
- [46] M. G. Tucker, D. A. Keen, M. T. Dove, A. L. Goodwin, and Q. Hui, RMCProfile: Reverse Monte Carlo for polycrystalline materials, *J. Phys.: Condens. Matter* **19**, 335218 (2007).
- [47] A. K. Soper, GudrunN and GudrunX, Tech. Rep. RAL-TR 13 (Rutherford Appleton Laboratory, 2012).
- [48] D. A. Keen, A comparison of various commonly used correlation functions for describing total scattering, *J. Appl. Crystallogr.* **34**, 172 (2001).
- [49] I. T. Todorov, W. Smith, K. Trachenko, and M. T. Dove, DL_POLY_3: New dimensions in molecular dynamics simulations via massive parallelism, *J. Mater. Chem.* **16**, 1911 (2006).
- [50] J. D. Gale, GULP: A computer program for the symmetry-adapted simulation of solids, *J. Chem. Soc., Faraday Trans.* **93**, 629 (1997).
- [51] J. D. Gale and A. L. Rohl, The General Utility Lattice Program (GULP), *Mol. Simul.* **29**, 291 (2003).
- [52] L. H. N. Rimmer and M. T. Dove, Simulation study of negative thermal expansion in yttrium tungstate $Y_2W_3O_{12}$, *J. Phys.: Condens. Matter* **27**, 185401 (2015).
- [53] M. G. Tucker, M. T. Dove, and D. A. Keen, Application of the reverse Monte Carlo method to crystalline materials, *J. Appl. Crystallogr.* **34**, 630 (2001).
- [54] M. T. Dove, M. G. Tucker, and D. A. Keen, Neutron total scattering method: Simultaneous determination of long-range and short-range order in disordered materials, *European J. Mineral.* **14**, 331 (2002).
- [55] D. A. Keen, M. G. Tucker, and M. T. Dove, Reverse Monte Carlo modeling of crystalline disorder, *J. Phys.: Condens. Matter* **17**, S15 (2005).
- [56] The recent study of Wendt *et al.* [26] reports two anomalous findings, first that the mean F–F distance shrinks with increasing temperature, and second that the integrated area of the second F–F peak in the PDF decreases with temperature. In both cases these are contrary to what we have found. These two anomalous results may reflect the limitations of analysis of the PDF alone, without the support of a model. As the F–F peak broadens with temperature, the data become increasingly noisy, and the pair density within any fixed r range will necessarily decrease. Furthermore, the analysis may also be affected by artifacts associated with untreated truncation effects at the maximum observable value of Q . Such problems highlight the value of making use of modeling approaches such as RMC, where the atomic model imposes reasonable physical constraints on the data analysis. The atomistic configuration generated by RMC has no ambiguity in assigning pair density where peaks are very broad or overlap, such as the 4 Å peak here, which encompasses both Sc–Sc and F–F pairs. Figures S7–S9 in the Supplemental Material [26] show the RMC-derived decomposition of the PDF into contributions from individual atomic pairs.
- [57] H. Fang, M. T. Dove, L. H. N. Rimmer, and A. J. Misquitta, Simulation study of pressure and temperature dependence of the negative thermal expansion in $Zn(CN)_2$, *Phys. Rev. B* **88**, 104306 (2013).
- [58] K. S. Aleksandrov, V. N. Voronov, A. N. Vtyurin, S. V. Goryainov, N. G. Zamkova, V. I. Zinenko, and A. S. Krylov, Lattice dynamics and hydrostatic-pressure-induced phase transitions in ScF_3 , *J. Exp. Theor. Phys.* **94**, 977 (2002).
- [59] S. A. Wells, M. T. Dove, and M. G. Tucker, Finding best-fit polyhedral rotations with geometric algebra, *J. Phys.: Condens. Matter* **14**, 4567 (2002).
- [60] S. A. Wells, M. T. Dove, M. G. Tucker, and K. Trachenko, Real-space rigid-unit-mode analysis of dynamic disorder in quartz, cristobalite and amorphous silica, *J. Phys.: Condens. Matter* **14**, 4645 (2002).
- [61] S. A. Wells, M. T. Dove, and M. G. Tucker, Reverse Monte Carlo with geometric analysis – RMC + GA, *J. Appl. Crystallogr.* **37**, 536 (2004).
- [62] In Fig. 4(a) the sizes of the fluctuations of the ScF_6 orientations and F–Sc–F angles are similar, but in Fig. 4(b) the GASP analysis suggest that the motions of the F atoms associated with bond bending are rather larger than from rotations of the octahedra. These results are actually consistent with each other: The contribution to M from the octahedral rotation will come from three axes, but there are 12 bending angles associated with deformation of the octahedra.
- [63] Q. Hui, M. G. Tucker, M. T. Dove, S. A. Wells, and D. A. Keen, Total scattering and reverse Monte Carlo study of the 105 K displacive phase transition in strontium titanate, *J. Phys.: Condens. Matter* **17**, S111 (2005).
- [64] But it would be wrong to say that it *is* the limiting case, because the model, being a simplified model, is not an exact representation of the actual material. In particular, the division between the three types of motion is not exactly the same. What we are demonstrating is that even in the limit of fairly flexible octahedra the GASP method will still identify whole-body rotations.
- [65] There are two important points to highlight in the two diagrams in Fig. 4. The first is that the angular fluctuations in (a) increase linearly with temperature, in line with expectations from classical quasiharmonic lattice dynamics. Second is that the distribution of atomic motion over the three components in (b) is more-or-less constant with temperature, reflecting phonon eigenvectors and again being fully consistent with classical quasiharmonic lattice dynamics. In particular, although thermal motion is large at the higher temperature, it does not lead to any breakdown of the classical picture, contrary to the opinion expressed in Ref. [26].
- [66] We consider models in which the Sc–F bond is the sole rigid entity, with complete flexibility of the ScF_6 octahedra, as for example in Ref. [26], to be overflexible and unable to provide useful insights, not least because such models will predict the wrong signs of the Grüneisen parameters for many phonon modes. A similar situation was discussed with regard to NTE

- in Cu_2O in Ref. [84], where the true rigid entity is the linear O–Cu–O trimer, and models that consider only the O–Cu bonds as the rigid entities are too flexible.
- [67] P. Lazar, T. Bučko, and J. Hafner, Negative thermal expansion of ScF_3 : Insights from density-functional molecular dynamics in the isothermal-isobaric ensemble, *Phys. Rev. B* **92**, 224302 (2015).
- [68] D. Bocharov, Y. Rafalskij, M. Krack, M. Putnina, and A. Kuzmin, Negative thermal expansion of ScF_3 : First principles vs empirical molecular dynamics, *IOP Conf. Ser.: Mater. Sci. Eng.* **503**, 012001 (2019).
- [69] D. Bocharov, M. Krack, Yu. Rafalskij, A. Kuzmin, and J. Purans, *Ab initio* molecular dynamics simulations of negative thermal expansion in ScF_3 : The effect of the supercell size, *Comput. Mater. Sci.* **171**, 109198 (2020).
- [70] A. van Roekeghem, J. Carrete, and N. Mingo, Anomalous thermal conductivity and suppression of negative thermal expansion in ScF_3 , *Phys. Rev. B* **94**, 020303(R) (2016).
- [71] In common usage, the term *quasiharmonic* model considers the effect of changes in volume on the phonon frequencies through the consequent changes in harmonic force constants, giving new harmonic phonon frequencies as modified by the anharmonic coupling of force constants to volume. The term *renormalized phonon* model considers how a renormalized harmonic Hamiltonian can result from a mean-field treatment of the anharmonic interactions between phonons, typically focusing on the fourth-order interactions.
- [72] M. T. Dove, *Introduction to Lattice Dynamics* (Cambridge University Press, Cambridge, 2009).
- [73] Importantly, the reverse Monte Carlo method is indeed capable of generating such distributions in cases where they genuinely exist; one clear example is that of the cubic phase of cristobalite [85].
- [74] J. Du, A. E. Phillips, D. C. Arnold, D. A. Keen, M. G. Tucker, and M. T. Dove, Structural study of bismuth ferrite BiFeO_3 by neutron total scattering and the reverse Monte Carlo method, *Phys. Rev. B* **100**, 104111 (2019).
- [75] M. T. Dove, A. P. Giddy, and V. Heine, On the application of mean-field and Landau theory to displacive phase transitions, *Ferroelectrics* **136**, 33 (1992).
- [76] M. T. Dove, V. Heine, and K. D. Hammonds, Rigid unit modes in framework silicates, *Mineral. Mag.* **59**, 629 (1995).
- [77] M. T. Dove, M. Gambhir, K. D. Hammonds, V. Heine, and A. K. A. Pryde, Distortions of framework structures, *Phase Transitions* **58**, 121 (1996).
- [78] M. Gambhir, V. Heine, and M. T. Dove, A one-parameter model of a rigid-unit structure, *Phase Transitions* **61**, 125 (1997).
- [79] M. T. Dove, M. Gambhir, and V. Heine, Anatomy of a structural phase transition: Theoretical analysis of the displacive phase transition in quartz and other silicates, *Phys. Chem. Miner.* **26**, 344 (1999).
- [80] A. V. Tkachenko and I. A. Zaliznyak, Criticality, entropic elasticity, and negative thermal expansion of a coulomb floppy network: ScF_3 -inspired theory for a class of ionic solids, [arXiv:1908.11643](https://arxiv.org/abs/1908.11643).
- [81] L. Wang, C. Wang, Y. Sun, K. Shi, S. Deng, H. Lu, P. Hu, and X. Zhang, Metal fluorides, a new family of negative thermal expansion materials, *J. Materiomics* **1**, 106 (2015).
- [82] The research group of Angus Wilkinson has explored several fluorides with crystal structures analogous to ScF_3 , including materials with various levels of doping [86–90]. Many examples display phase transitions involving rotations of octahedra and which appear to be continuous (second-order). These phase transitions will be accompanied by the softening of the RUM phonons on cooling towards the transition temperature, through the types of anharmonic interactions discussed in this paper as described by Eq. (1). We have shown that such a variation of the renormalized phonon frequency with temperature will lead to a reduction, or even elimination, of NTE [31], as also demonstrated in recent calculations [32, 70].
- [83] M. T. Dove, M. G. Tucker, T. Zhang, A. E. Phillips, and J. Du, Structural origin of negative thermal expansion in ScF_3 (STFC ISIS Neutron and Muon Source, 2015), doi:[10.5286/ISIS.E.RB1510519](https://doi.org/10.5286/ISIS.E.RB1510519).
- [84] L. H. N. Rimmer, M. T. Dove, B. Winkler, D. J. Wilson, K. Refson, and A. L. Goodwin, Framework flexibility and the negative thermal expansion mechanism of copper(I) oxide Cu_2O , *Phys. Rev. B* **89**, 214115 (2014).
- [85] M. G. Tucker, M. P. Squires, M. T. Dove, and D. A. Keen, Dynamic structural disorder in cristobalite: Neutron total scattering measurement and reverse Monte Carlo modeling, *J. Phys.: Condens. Matter* **13**, 403 (2000).
- [86] C. R. Morelock, B. K. Greve, L. C. Gallington, K. W. Chapman, and A. P. Wilkinson, Negative thermal expansion and compressibility of $\text{Sc}_{1-x}\text{Y}_x\text{F}_3$ ($x \leq 0.25$), *J. Appl. Phys.* **114**, 213501 (2013).
- [87] C. R. Morelock, J. C. Hancock, and A. P. Wilkinson, Thermal expansion and phase transitions of $\alpha\text{-AlF}_3$, *J. Solid State Chem.* **219**, 143 (2014).
- [88] J. C. Hancock, K. W. Chapman, G. J. Halder, C. R. Morelock, B. S. Kaplan, L. C. Gallington, A. Bongiorno, C. Han, Si Zhou, and A. P. Wilkinson, Large negative thermal expansion and anomalous behavior on compression in cubic ReO_3 -type $\text{A}^{\text{II}}\text{B}^{\text{IV}}\text{F}_6$: CaZrF_6 and CaHfF_6 , *Chem. Mater.* **27**, 3912 (2015).
- [89] C. R. Morelock, L. C. Gallington, and A. P. Wilkinson, Solid solubility, phase transitions, thermal expansion, and compressibility in $\text{Sc}_{1-x}\text{Al}_x\text{F}_3$, *J. Solid State Chem.* **222**, 96 (2015).
- [90] B. R. Hester and A. P. Wilkinson, Negative thermal expansion, response to pressure and phase transitions in CaTiF_6 , *Inorg. Chem.* **57**, 11275 (2018).